1999

Magnetic Resonance Imaging Analysis of Molecular Mobility during Dissolution of Poly(vinyl alcohol) in Water

Balaji Narasimhan, *Rutgers University - New Brunswick/Piscataway*
J. E.M. Snaar, *University of Nottingham*
R. W. Bowtell, *University of Nottingham*
S. Morgan, *University of Nottingham*
C. D. Melia, *University of Nottingham*, et al.

Magnetic Resonance Imaging Analysis of Molecular Mobility during Dissolution of Poly(vinyl alcohol) in Water

B. Narasimhan,*,† J. E. M. Snaar,‡ R. W. Bowtell,‡ S. Morgan,§ C. D. Melia,§ and N. A. Peppas⊥

Department of Chemical and Biochemical Engineering, Rutgers University, 98 Brett Road, Piscataway, New Jersey 08854-8058; Magnetic Resonance Centre and Department of Physics and Department of Pharmaceutical Sciences, University of Nottingham, University Park, Nottingham, NG7 2RD, UK; and School of Chemical Engineering, Purdue University, West Lafayette, Indiana 47907-1283

Received September 1, 1998; Revised Manuscript Received November 30, 1998

ABSTRACT: Magnetic resonance imaging is used to study changing microstructure and molecular motion during dissolution of poly(vinyl alcohol) (PVA) in water. One-dimensional water concentration profiles were measured as a function of distance from the polymer−solvent interface. Diffusion-weighted profiles were used to calculate the spatial variation of the self-diffusion coefficient of water. The results indicate that diffusion coefficient values decrease toward the glassy core of the polymer. Self-diffusion coefficient values within the dissolving polymer increase with increasing dissolution time, while those near the polymer−solvent interface remain fairly constant. The effect of PVA molecular weight on the dissolution mechanism was investigated, with $\bar{M}_n$ varying between 35 740 and 133 000. Comparisons were made with a mathematical model for polymer dissolution. The water concentration profiles predicted by the model are qualitatively consistent with the experimentally obtained profiles. In addition, the scaling laws proposed in the model for the polymer diffusion coefficients are verified. The calculated polymer diffusion coefficients (based on the experimental data) yield D (polymer self-diffusion coefficient) $\sim M^{-1.9}$ (theory predicts an exponent of −2) and $D \sim M^{-0.6}$ (theory predicts an exponent of −0.5) near the glassy−rubbery and the rubbery−solvent interfaces, respectively, providing supporting evidence for the hypothesis that phenomena such as reptation are important near the glassy−rubbery interface while Zimm-type diffusion occurs near the polymer−solvent interface. The results also point to the existence of a change in the mode of diffusion as solvent penetrates into the polymer.

Introduction

Polymer dissolution is an important phenomenon in polymer science and engineering. For example, in microlithography, selectively irradiated regions of a photosensitive polymer are dissolved in appropriate solvents to obtain desired circuit patterns.[1] In the field of controlled drug release, zero-order drug release systems have been designed[2] by rendering the polymer dissolution phenomenon as the controlling step in the release process. Polymer dissolution also finds applications in membrane science,[3] treatment of unsorted plastics for recycling,[4] the semiconductor industry,[5] and packaging.[6]

The dissolution of a polymer in a solvent involves two transport processes, namely, solvent diffusion and chain disentanglement. When an uncrosslinked, amorphous, glassy polymer is brought in contact with a thermodynamically compatible solvent, the latter diffuses into the polymer, and when the solvent concentration in the swollen polymer reaches a critical value, chain disentanglement begins to dominate and eventually the polymer is dissolved. Ueberreiter and co-workers[7−9] summarized the various types of dissolution and the surface structure of glassy polymers during dissolution. Important parameters such as the polymer molecular weight, the solvent diffusion coefficient, the gel layer thickness, the rate of agitation, and temperature were identified. Since then, various mathematical models have been proposed to understand polymer dissolution.

The approaches to model polymer dissolution are based[10] on (i) phenomenological models and Fickian equations,[11−14] (ii) models with external mass transfer as the controlling resistance to dissolution,[15] (iii) stress relaxation,[16,17] and (iv) anomalous transport models for solvent transport and scaling laws for chain disentanglement.[18−21] In this work, a model based on anomalous transport and scaling laws developed by us[20,21] will be analyzed, and comparisons will be made between the model predictions and experimental results.

For the comparison between models and experimental dissolution behavior, the techniques employed thus far include laser interferometry,[22−25] differential refractometry,[8] optical microscopy,[26] ellipsometry,[27] and spin echo NMR.[19] In this work, magnetic resonance imaging (MRI) is used to study the dissolution of swollen, noncrystalline poly(vinyl alcohol) (PVA) in water. MRI has been widely applied in medical diagnostics,[28] biological imaging,[29,30] and polymer science.[29−34] MRI provides three-dimensional information in a nondestructive manner. The technique is molecule specific and can also yield information on local variation in properties. The concentration in any region can be spatially resolved, thus removing limitations of sample geometry. The present work seeks to demonstrate the feasibility of using MRI to effectively study the mechanism of polymer dissolution. In addition, it will be shown that MRI is a useful tool to delineate the importance of different regimes during a diffusion-type process in polymeric systems. This idea is especially attractive for

* To whom all correspondence should be addressed.
† Rutgers University.
‡ Magnetic Resonance Centre and Department of Physics, University of Nottingham.
§ Department of Pharmaceutical Sciences, University of Nottingham.
⊥ Purdue University.

10.1021/ma981382k CCC: $18.00
Published on Web 01/14/1999

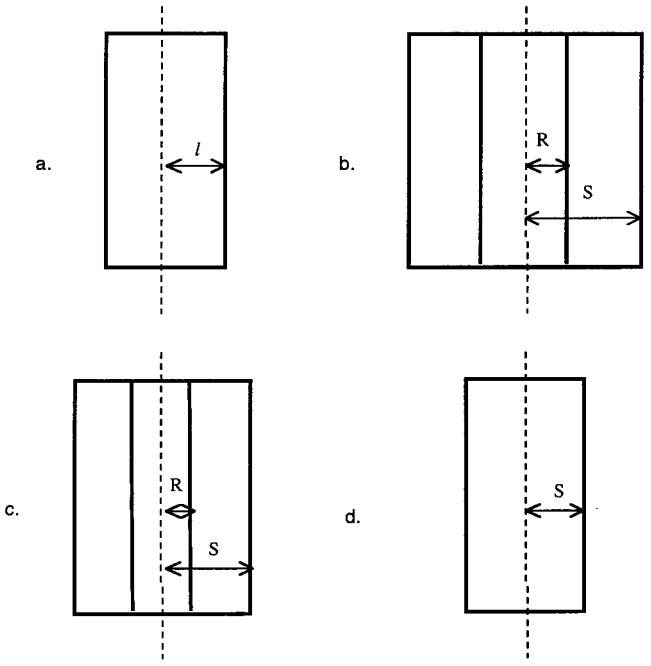

Figure 1. Schematic representation of a one-dimensional solvent diffusion and polymer dissolution process: (a) initial slab of thickness 2*l*; (b) initial swelling step showing the increasing position of the rubbery−solvent interface (S) and the decreasing position of the glassy−rubbery interface (R); (c) onset of the dissolution step showing the decreasing position of the interface S along with the decreasing position of the interface R; and (d) final dissolution step where the slab has been transformed into a rubbery material (disappearance of interface R) and the position of interface S still decreases.

the design of drug delivery systems based on dissolving polymer carriers.[35]

Polymer Dissolution Model

The important features of the dissolution model of Narasimhan and Peppas[20,21] are summarized in this section. The physical mechanism of the dissolution phenomenon is depicted in Figure 1. During the initial stage of the dissolution process, a glassy polymer of thickness 2*l* starts swelling due to the penetration of the solvent into it and the simultaneous transition from the glassy to the rubbery state. Thus, two distinct fronts are observed: a swelling interface at position *R* and a polymer/solvent interface at position *S*. Front *R* moves inward while front *S* moves outward. When the concentration of the penetrant in the polymer exceeds a critical value, macromolecular disentanglement begins. After the concentration exceeds the critical value, true dissolution commences. After macromolecular disentanglement is complete, the polymer is dissolved. During this time, front *R* continues to move toward the center of the slab, while front *S* moves inward as well. After the disappearance of the glassy core, only front *S* exists, and it continues to move inward toward the center of the slab until the entire polymer is dissolved.

The entire concentration field was divided into three regimes. The swollen polymer (i.e., the region $R < x < S$ in Figure 1) was defined as the "concentrated" regime. A diffusion boundary layer adjacent to the rubbery−solvent interface, *S*, through which the disentangled chains diffuse was assumed. The diffusion boundary layer was defined as the "semidilute" regime and has a constant thickness, δ. When the polymer is fully dissolved, the disentangled chains move freely in the solvent and exhibit Brownian motion. This region was referred to as the "dilute" regime.

The solvent flux into a glassy polymer in the concentrated regime was expressed as the sum of a diffusional contribution and an osmotic pressure term (arising from linear irreversible thermodynamics).[21] The osmotic pressure term was related to the viscoelastic stress of the polymer by a momentum balance. The appropriate governing equations in one dimension for the concentrated regime become

$$\frac{\partial v_1}{\partial t} = \frac{\partial}{\partial x}\left[D_{12}\frac{\partial v_1}{\partial x}\right] + \frac{\partial}{\partial x}\left[\frac{D_{12}\bar{V}_1 v_1}{RT(1-v_1)(1-2\chi v_1)}\frac{\partial \sigma_{xx}}{\partial x}\right] \quad (1)$$

$$\frac{\partial \sigma_{xx}}{\partial t} = -\frac{\sigma_{xx}}{\eta/E} + \frac{E}{(1-v_1)^2}\frac{\partial v_1}{\partial t} \quad (2)$$

Here v_1 is the volume fraction of solvent in the swollen polymer, D_{12} is the solvent−polymer mutual diffusion coefficient, $\bar{V}_1$ is the molar volume of the solvent, *R* is the gas constant, *T* is the temperature, χ is the solvent−polymer interaction parameter, σ_{xx} is the *xx* component of the viscoelastic stress tensor of the polymer, η is the viscosity of the polymer, and *E* is the tensile modulus of the polymer. The polymer viscosity depends on the penetrant concentration in the following manner:

$$\eta = \eta_0 \exp(-a v_1) \quad (3)$$

It must be noted here that the viscoelastic stress of the polymer was modeled using a Maxwell model. In principle, any constitutive equation may be used.

The model equation in the semidilute regime was written as

$$\frac{\partial v_2}{\partial t} = \frac{\partial}{\partial x}\left[D_p\frac{\partial v_2}{\partial x}\right] - \frac{dS}{dt}\frac{\partial v_2}{\partial x} \quad (4)$$

Here v_2 is the polymer volume fraction, *S* is the position of the rubbery−solvent interface, and D_p is the polymer self-diffusion coefficient in the semidilute regime. Appropriate initial and boundary conditions were written for each of the above system of equations.

The mutual diffusion coefficient, D_{12}, was expressed as[36]

$$D_{12} = \frac{D_1\rho_1\rho_2}{RT}\hat{V}_2\frac{\partial \mu_1}{\partial \rho_1} \quad (5)$$

Here, D_1 is the self-diffusion coefficient of the solvent, ρ_1 and ρ_2 are the weights per unit volume of solvent and polymer, respectively, $\hat{V}_2$ is the specific molar volume of the polymer, and μ_1 is the chemical potential of the solvent. Using the classical Flory−Rehner treatment[37] that considers entanglements, the solvent chemical potential can be obtained as

$$\frac{\mu_1 - \mu_1^0}{RT} = \ln(v_1) + 1 - v_1 + \chi(1-v_1)^2 + \bar{V}_1\rho_2\left(\frac{2}{M_e} - \frac{1}{\bar{M}_n}\right)\left(\frac{2}{1-v_1} - (1-v_1)\right) \quad (6)$$

Here M_e is the entanglement molecular weight of the polymer. From eqs 5 and 6, the mutual diffusion coefficient can be obtained in terms of D_1. Vrentas and Vrentas[38] have obtained the relationship between D_{12}

and D_2 (the self-diffusion coefficient of the polymer) as

$$D_{12} = \frac{QD_1}{\alpha v_1^{\,2} + 1} \tag{7}$$

$$\alpha = \frac{M_1}{M_2}\frac{\hat{V}_1^{\,0}}{\hat{V}_{20}}\frac{D_1}{D_2} \quad \text{and} \quad Q = \frac{\rho_1}{RT}\frac{\partial \mu_1}{\partial \rho_1} \tag{8}$$

Here, $\hat{V}_1^0$ is the specific volume of the solvent and $\hat{V}_{20}$ is the partial specific volume of the polymer. It is to be noted that the relationship between D_{12} and D_p, the polymer self-diffusion coefficient in the semidilute regime, would also be given by eqs 7 and 8. Vrentas and Vrentas[39] have applied this model to calculate self-diffusion coefficients from mutual diffusion coefficients for different polymer−solvent systems.

The model assumes that the mode of transport in the concentrated regime is governed by reptation,[40,41] and hence the molecular weight dependence of the diffusion coefficient is given by $D_2 \sim M^{-2}$. The diffusion in the semidilute regime is modeled as a Zimm process[42] and yields $D_p \sim M^{-0.5}$. The diffusion coefficients in the model were predicted using theories of reptation, and the Zimm analysis for the polymer self-diffusion coefficients and the disentanglement rate of a polymer chain was expressed as the ratio between the radius of gyration of the polymer and its reptation time. The model equations were then numerically solved using an implicit finite difference algorithm.

Experimental Section

Materials. PVA grades (Elvanol grades 85-82, 90-50, and HV (with degrees of hydrolysis exceeding 99.2%), E. I. duPont de Nemours, Wilmington, DE; PVA (MW = 133 000, degree of hydrolysis exceeding 99.2%, polydispersity index = 2.10), Polysciences, Philadelphia, PA) were used for the experiments. The molecular weights of these grades were determined as $\bar{M}_n$ = 48 240, 35 740, and 64 000, respectively, with corresponding polydispersity indices of 2.16, 2.15, and 2.02, and were obtained by gel permeation chromatography (GPC) experiments (Lark Enterprises, Webster, MA). The detector used was a Waters 410 differential refractive index detector along with a Shodex aqueous GPC column. The eluent used was 0.1 N $NaNO_3$, and the rate of elution was 1 mL/min at 45 °C. A monodisperse PVA (Eastman Kodak, Rochester, NY) sample of known molecular weight was used as the standard.

PVA solutions (10% w/v) were prepared[43] by dissolving dry PVA in deionized water at 90 °C for 6 h. The polymer films were cast on glass plates of size 8 × 8 cm^2. The glass plates were initially treated with a commercial siliconizing agent (Prosil-28, PCR Inc., Gainesville, FL) to prevent the films from sticking to the glass surface and to facilitate easy removal. A 1% solution of Prosil-28 in deionized water was prepared. The glass plates were cleaned thoroughly before surface treatment. They were then dipped three or four times into a beaker containing this solution and then placed in an oven at a constant temperature of 100 °C for 10 min. The siliconized glass plates were then used for casting the films. Siliconizing prevents the sticking of the films to the glass plates, because the hydrophobic groups of the siliconizing agent cause repulsion of the −OH groups of the PVA from the glass surface.

The PVA solution was poured onto the glass plates and spread uniformly over the surface using a glass rod. It was then allowed to dry at a constant temperature of 25 °C in a glass dish placed in a water bath for 7 days. The films were then removed and were found to have thicknesses of about 0.1 mm. The films were then brought into contact with liquid nitrogen and then placed in a freezer for 48 h. The film was then size reduced (particle size ranging between 200 and 800 μm), compressed (using a force of 2000 lb), and machined into tablets.

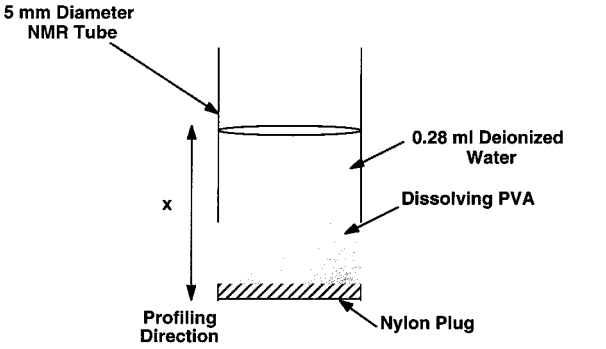

Figure 2. The PVA sample and the nylon plug placed in the NMR tube. One-dimensional images, showing the variation of signal in the *x*-direction, are obtained.

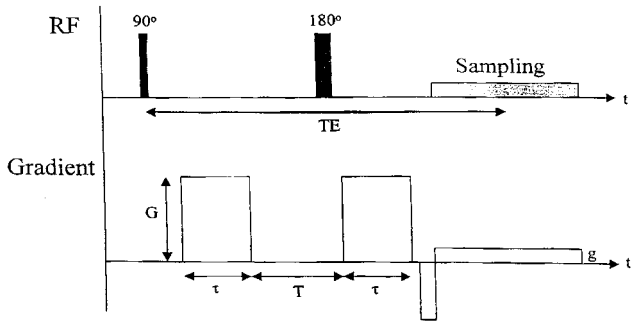

Figure 3. Timing diagram for the one-dimensional imaging sequence used.

Differential scanning calorimetry (DSC, TA Instruments, New Castle, DE) was used to measure the glass transition temperature, T_g, and the degree of crystallinity of the polymer sample. In a typical experiment, about 5 mg of the polymer sample was placed in a sample pan and heated at 2.5 °C/min. All the DSC studies were conducted under a constant purge of nitrogen. The quenching technique resulted in samples that had degrees of crystallinities not exceeding 5%.

MRI. Flat-faced PVA tablets of 4.2 mm diameter and 2−2.5 mm thickness prepared by the technique described in the previous section were fixed to a 4.2 mm diameter nylon substrate plug using a small amount of cyanoacrylate adhesive. The plug was then glued inside a 5 mm NMR tube, with both the PVA tablet and the nylon making a tight fit inside the tube. The tube was filled with approximately 0.28 mL of deionized water and placed in the magnet (Figure 2). One-dimensional imaging was carried out using an NMR[44] microscope interfaced with a 11.7 T, 89 mm bore superconductive magnet, providing a proton resonance frequency of 500 MHz. A 6 mm diameter RF saddle coil and a highly efficient gradient coil,[45] capable of generating 1.73 T m^{-1} A^{-1}, were used.

The pulse sequence used for imaging[46] is shown in Figure 3. A spin echo is generated by the 90° and 180° RF pulses at time TE. This coincides with the gradient echo formed under the read gradient, *g*. Diffusion weighting is provided by a pair of gradient pulses of strength *G* applied along the same axis as the read gradient, on either side of the 180° RF pulse. The resultant attenuation of the NMR signal for this sequence depends on the self-diffusion coefficient, *D*, and is given by

$$S/S_0 = \exp[-(\gamma G\tau)^2(^2/_3\tau + T)D] \tag{9}$$

Here, *S* is the attenuated magnetization, S_0 is the equilibrium value, γ is the gyromagnetic ratio, *G* is the magnetic field gradient strength, and τ and *T* are the diffusion-weighting gradient pulse duration and separation times, respectively.

Thus, a plot of the natural logarithm of the normalized signal intensity versus $b = (\gamma G\tau)^2(2\tau/3 + T)$ is a straight line with slope $-D$. In the sequence of Figure 3, the NMR signal is sampled in the presence of the read gradient and then Fourier transformed to yield a diffusion-weighted, one-dimensional profile of the sample. A set of such profiles is built up by repeating the experiment using different values of G. A one-dimensional profile showing the variation of self-diffusion coefficient with position can then be generated by fitting the signal variation to eq 9 on a point by point basis.

One-dimensional profiles of 29 μm resolution, showing the variation of water concentration or self-diffusion coefficient, were generated after various dissolution times using the above spin echo sequence (repetition time, TR = 5 s; echo time, TE = 2.75 ms, $G_{max} = 9.8$ T m^{-1}; $g = 0.8$ T m^{-1}; $\tau = 564$ μs; signal sampled for 1.024 ms; and field of view = 7.42 mm). With the diffusion encoding gradients switched off, the resulting profile is mainly spin density weighted, thus showing the variation of water concentration, since in all samples T_2 is of the order of 10 ms and T_1 is approximately 1 s. Such concentration profiles were measured at approximately 3 min intervals during the first 30 min of dissolution and then at times of 1 and 2 h of dissolution. Each profile was obtained from an average of eight experiments, giving a total acquisition time of 40 s. Diffusion measurements were made after 30 min, 1 h, and 2 h, using nine profiles generated with different diffusion weightings (gradient attenuation varying from 10^3 to 2.5 s mm^{-2}). The total time required to make a diffusion measurement was 6 min. All measurements were made at an average temperature of 19 ± 1 °C.

Results and Discussion

The simulations were performed using water−PVA as a model system, in which relevant thermodynamic and structural parameters at 19 °C were determined independently. The water−PVA interaction parameter,[47] χ, was 0.49. The interfacial concentration, $v_{1,eq}$, was calculated using the Flory−Rehner theory (eq 6) for PVA (for example, $v_{1,eq} = 0.814$ for PVA of molecular weight 48 240). The thickness of the diffusion boundary layer was chosen[48] to be 5% of the initial half thickness of the slab. The modulus, E, was taken as 3×10^8 Pa, and the preexponential factor for the viscosity (see eq 3) was chosen as 25. Exact expressions[20] were used to calculate the reptation time, the disentanglement rate, and the Zimm diffusion coefficient.

Equations 1 and 2 represent a system of two coupled, nonlinear partial differential equations. The solution of the above system of equations would generate the solvent concentration profile in the rubbery region of the polymer, the polymer concentration profile in the boundary layer, and the temporal evolution of the two moving boundaries. The concentration profiles can be integrated to obtain the mass of the polymer dissolved as a function of time. The moving boundary problem was transformed into a fixed boundary problem by using "front fixing" techniques[49] that utilize a new set of space coordinates. A fully implicit backward time centered space finite difference technique was utilized to transform the set of differential equations to a set of nonlinear algebraic equations at each time step. The resulting system was solved by using the Thomas algorithm.[50]

Concentration profiles for water transport through noncrystalline PVA (= 35 740, 48 240, 64 000, and 133 000) as a function of dimensionless position, ξ_1, are shown in Figure 4a−d. These are results of the simulations, and the concentration profiles have been calculated by using the Thomas algorithm. The fraction of PVA dissolved as a function of time can be calculated using the following expression:

$$\frac{M(t)}{M_0} = \int_0^t \frac{1}{(S-R)^2}\left(-D_{12}\frac{\partial v_2}{\partial \xi_1}\right)_{\xi_1=1} \mathrm{d}t \qquad (10)$$

Here, ξ_1 is a normalized position, and $\xi_1 = 1$ represents the rubbery−solvent interface. The fraction of PVA ($\bar{M}_n$ = 48 240) dissolved during the first 3 h of dissolution as a function of dissolution time is shown in Figure 5. In addition, the model can also predict the temporal evolution of the positions of the interfaces R and S.[21]

The water concentration profiles from the model predictions were compared to the profiles obtained from the imaging experiments. Figure 6a shows the experimentally measured solvent concentration profile in the polymer ($\bar{M}_n$ = 35 740) as a function of position and time. The PVA−substrate interface is at $x = 1$ mm, and the rubbery−solvent interface is initially at $x = 2.5$ mm. The steep profiles are indicative of a relaxation-controlled dissolution mechanism leading to case II type behavior. Mallapragada and Peppas[43] have shown that PVA dissolution in water follows case II type behavior over the range of molecular weights studied. The flat profiles in the rubbery region can be attributed to a very small diffusional resistance. The data indicate that the glassy core essentially behaves like an impervious wall, and as diffusional resistance increases, smoother concentration profiles are observed. This behavior is qualitatively similar to the one predicted by the model (see Figure 4a).

Figure 6b−d shows the measured water concentration profiles as a function of time for PVA of molecular weight 48 240, 64 000, and 133 000, respectively. Once again, the profiles show qualitatively consistent agreement with the model predictions (Figure 4b−d, respectively). It is to be noted that the profiles also show the accompanying swelling/disentanglement behavior of the polymer. As the molecular weight of the polymer increases, the rate of solvent penetration decreases. The amplitude is proportional to the solvent concentration in the polymer, and consequently, there is more solvent in the polymer in Figure 6a than in Figure 6b−d. This behavior is to be expected since increasing the polymer molecular weight decreases the swelling.

Figure 7 shows the spatial variation of the water self-diffusion coefficient in PVA ($\bar{M}_n$ = 35 740) after 30 min of dissolution. This profile displays a sudden drop in the diffusion coefficient at the water/PVA interface and a gradual decrease in D_1 for greater penetration distances into the polymer. This decrease in the diffusion coefficient value suggests that different modes of mobility may be governing the process at different spatial points. The values of D_2 were calculated using eqs 5−8 and plotted as a function of dissolution time for dissolution of PVA ($\bar{M}_n$ = 35 740) (Figure 8). It is observed that the values near the PVA−nylon interface increase with time while those near the PVA−water interface do not appreciably change as a function of time. This is to be expected as polymer chain mobility near the PVA−nylon interface increases as more water penetrates into the polymer while the system at the PVA−water interface can be approximated as a dilute solution of polymer chains at all times. Similar behavior was observed for the other molecular weights studied.

The presence of a distribution of self-diffusion coefficients can be attributed to the decreased segmental

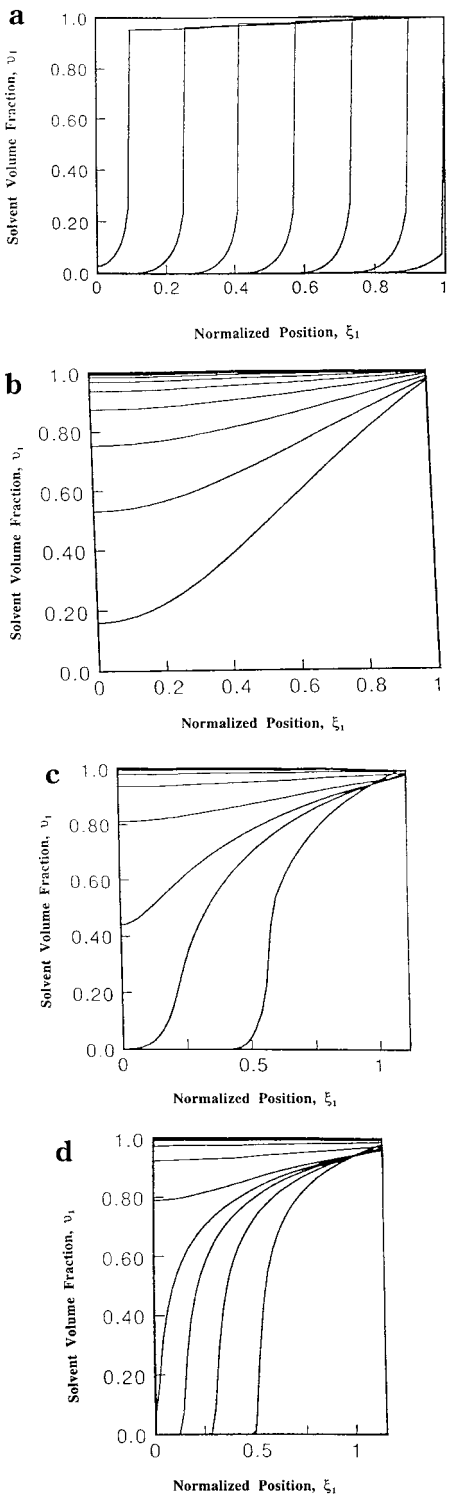

Figure 4. (a) Water volume fraction, v_1, as a function of normalized position, ξ_1. The PVA molecular weight was $\bar{M}_n$ = 35 740. The position $\xi_1 = 0$ is the center of the slab. The time increment starting from the first curve on the right is $\Delta t = 15$ min. (b) Water volume fraction, v_1, as a function of normalized position, ξ_1. The PVA molecular weight was $\bar{M}_n = 48\,240$. The position $\xi_1 = 0$ is the center of the slab. The time increment starting from the first curve on the right is $\Delta t = 15$ min. (c) Water volume fraction, v_1, as a function of normalized position, ξ_1. The PVA molecular weight was $\bar{M}_n = 64\,000$. The position $\xi_1 = 0$ is the center of the slab. The time increment starting from the first curve on the right is $\Delta t = 15$ min. (d) Water volume fraction, v_1, as a function of normalized position, ξ_1. The PVA molecular weight was $\bar{M}_n = 133\,000$. The position $\xi_1 = 0$ is the center of the slab. The time increment starting from the first curve on the right is $\Delta t = 15$ min.

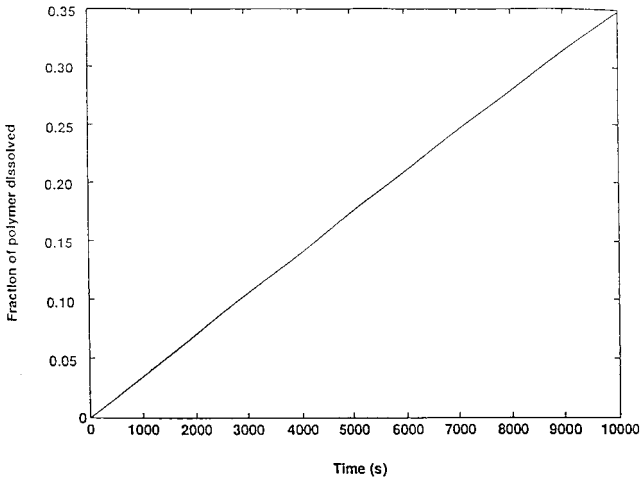

Figure 5. Fraction of PVA dissolved as a function of time. The polymer molecular weight was $\bar{M}_n = 48\,240$.

mobility of the polymer[51] toward the glassy core. The extremely limited mobility of the polymer chains near the glassy region hinders solvent transport, thereby decreasing the self-diffusion coefficient. It appears from the gradual decrease of the diffusion coefficient (see Figure 7) that the slope of the diffusivity profile may be less steep than would be expected for case II type behavior. This indicates that there is a gradual change in the mode of the diffusion process within the polymer as dissolution proceeds. It is interesting to observe that PVA dissolution in water does follow a linear relationship with time.[43] This behavior is also predicted by the model (Figure 5).

An important aspect to be noted in this analysis is that the range of the diffusion coefficients calculated for the polymer varied from about 10^{-13} to about 10^{-10} m^2/s. These numbers are consistent with the values reported by Tirrell[52] for diffusion coefficient values of polymers of comparable molecular weights by NMR techniques. The values vary by a factor of 4 or 5 from those obtained by IR[53] and small-angle neutron scattering[54] experiments.

The molecular weight dependence of the self-diffusion coefficients of the polymer was also investigated. The values were calculated at positions near the PVA−nylon interface as well as near the PVA−water interface. This is because the experiments seek to validate the model hypotheses that diffusion is reptation-dominated within the polymer while it is Zimm-type near the polymer−solvent interface. Accordingly, Figure 9 shows a log−log plot of the diffusion coefficient calculated from the measured NMR data near the PVA−nylon interface as a function of the polymer molecular weight. The slope of the straight line fit is −1.9, while reptation predicts a slope of −2. The values are in reasonable agreement, indicating the importance of phenomena like reptation well within the polymer during its dissolution. The diffusion coefficient near the PVA−water interface as a function of the polymer molecular weight is shown in the same figure (Figure 9). The slope of this line is −0.6, while the Zimm analysis predicts a slope of −0.5. Once again, the numbers seem to point toward the existence of Zimm-type diffusion phenomena near the polymer−solvent interface during dissolution. An intriguing indication is the possible existence of a change of mode of diffusion of the macromolecular chains as dissolution proceeds. This is clear from the completely different

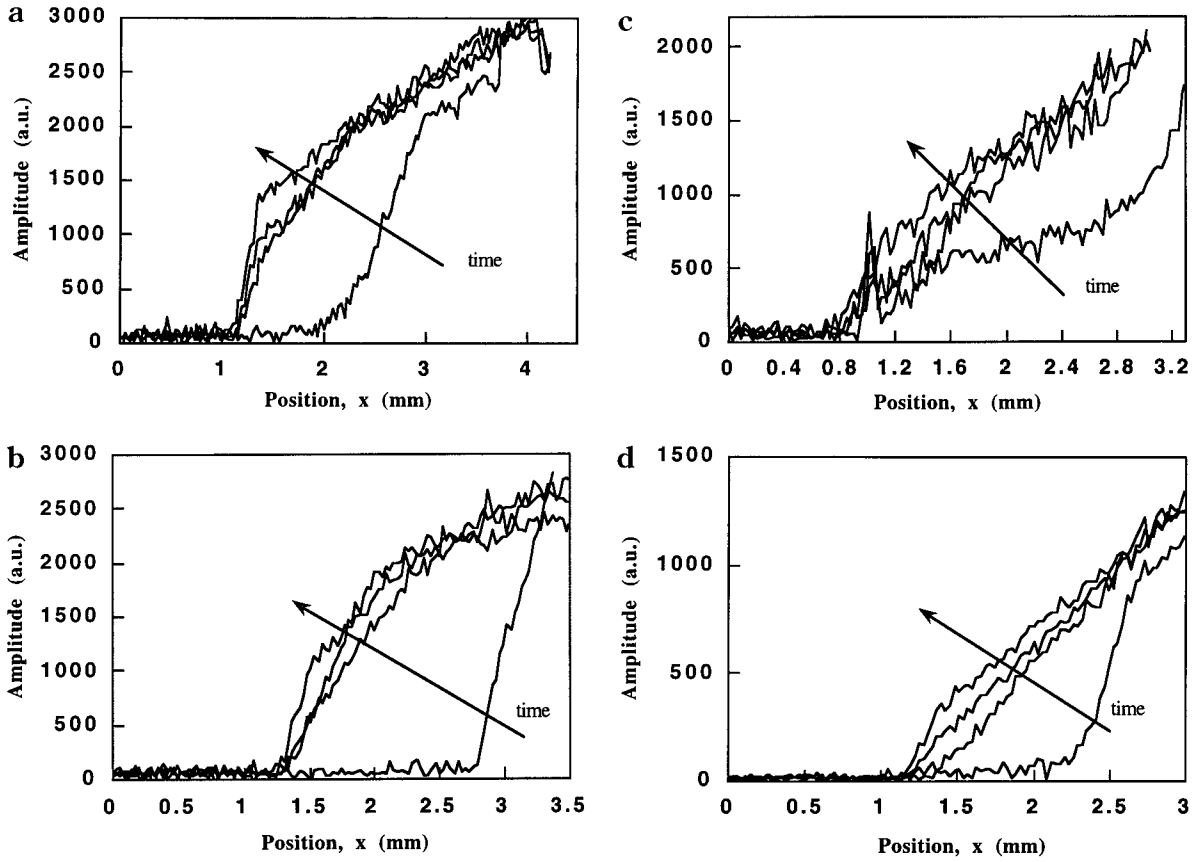

Figure 6. (a) One-dimensional water concentration profiles obtained during PVA ($\bar{M}_n$ = 35 740) dissolution using the spin echo sequence applied after varying times (2 min, 30 min, 1 h, and 2 h). The PVA−substrate interface is located at x = 1 mm, and the profile at positions greater than x = 4.3 mm, which shows the water layer on the surface, has been omitted for clarity. (b) One-dimensional water concentration profiles obtained during PVA ($\bar{M}_n$ = 48 240) dissolution using the spin echo sequence applied after varying times (2 min, 30 min, 1 h, and 2 h). The PVA−substrate interface is located at x = 1 mm, and the profile at positions greater than x = 3.5 mm, which shows the water layer on the surface, has been omitted for clarity. (c) One-dimensional water concentration profiles obtained during PVA ($\bar{M}_n$ = 64 000) dissolution using the spin echo sequence applied after varying times (2 min, 30 min, 1 h, and 2 h). The PVA−substrate interface is located at x = 1 mm, and the profile at positions greater than x = 3.3 mm, which shows the water layer on the surface, has been omitted for clarity. (d) One-dimensional water concentration profiles obtained during PVA ($\bar{M}_n$ = 133 000) dissolution using the spin echo sequence applied after varying times (2 min, 30 min, 1 h, and 2 h). The PVA−substrate interface is located at x = 1 mm, and the profile at positions greater than x = 3 mm, which shows the water layer on the surface, has been omitted for clarity.

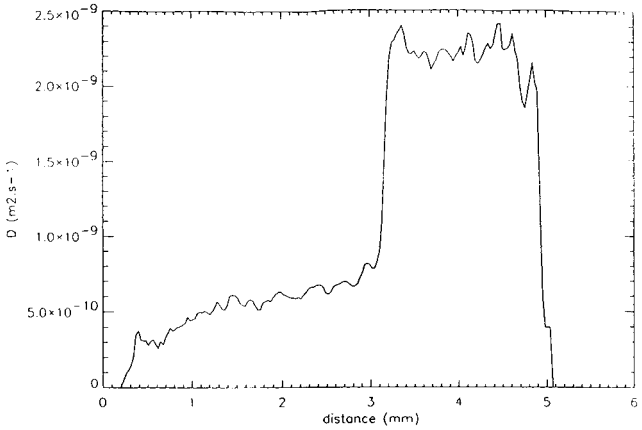

Figure 7. One-dimensional profile of the spatially varying water self-diffusion coefficient after 30 min of dissolution of PVA ($\bar{M}_n$ = 35 740).

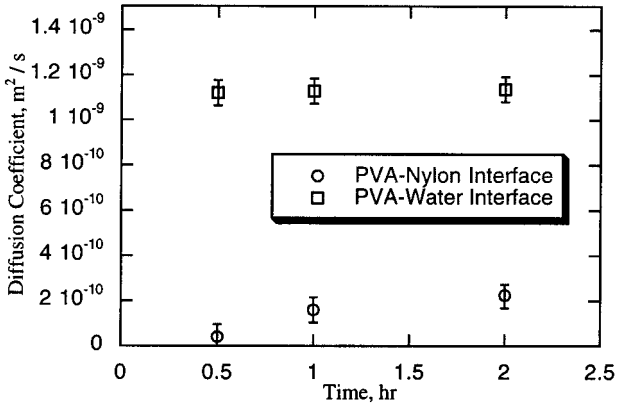

Figure 8. Diffusion coefficient, D_2, as a function of time at the PVA−substrate interface as well as at the PVA−water interface. The data are for a PVA sample of $\bar{M}_n$ = 35 740.

slopes (−1.9 and −0.6) obtained from the diffusion coefficient vs molecular weight data.

Conclusions

This study demonstrates the feasibility of using magnetic resonance imaging to study changing microstructure and molecular mobility during dissolution of polymers in solvents. Solvent concentration profiles as well as diffusion-weighted profiles to calculate the spatial variation of the self-diffusion coefficients can be obtained from the imaging experiments. These data were obtained in this study for uncrosslinked, noncrystalline PVA dissolution in water at 19 °C. The results

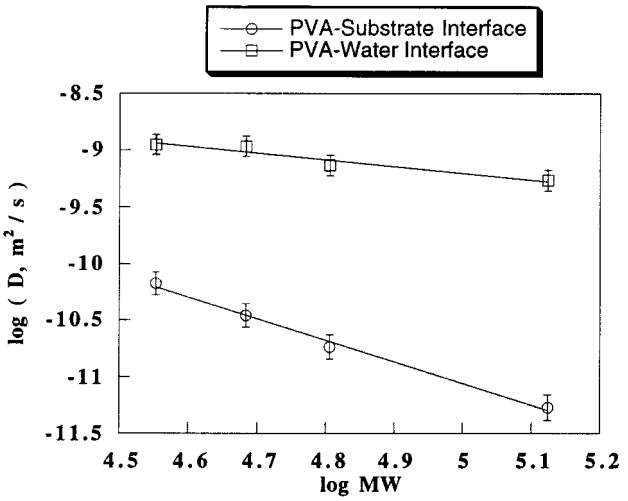

Figure 9. Molecular weight dependence of the polymer self-diffusion coefficient measured near the PVA−substrate interface and the PVA−water interface. The measurements were made after 30 min of dissolution of the polymer. The slopes of the straight lines are −0.6 and −1.9, respectively.

indicate that the diffusion coefficients decrease toward the glassy core of the polymer and also decrease as the polymer molecular weight is increased. Comparisons with a mathematical model for polymer dissolution showed that the predicted water profiles are qualitatively similar to the experimentally obtained profiles. In addition, the scaling laws proposed in the model for the diffusion coefficients were verified. The experiments seem to provide supporting evidence that phenomena such as reptation are important near the glassy−rubbery interface while Zimm-type diffusion occurs near the polymer−solvent interface.

Acknowledgment. This work was supported in part by Grant CTS-92-12482 from the National Science Foundation and EPSRC Grant GRIH96980. We thank Professor Surya K. Mallapragada of Iowa State University for useful discussions and suggestions.

References and Notes

(1) O'Brien, M. J.; Soane, D. S. Resists in Microlithography. In *Microelectronics Processing: Chemical Engineering Aspects*; Hess, D. W., Jensen, K. F., Eds.; Adv. Chem. Ser. 221; American Chemical Society: Washington, DC, 1989; pp 325−376.
(2) Narasimhan, B.; Peppas, N. A. *J. Pharm. Sci.* **1997**, *86*, 297.
(3) Tsay, C. S.; McHugh, A. J. *J. Polym. Sci., Polym. Phys. Ed.* **1990**, *28*, 1327.
(4) Nauman, E. B.; Lynch, J. C. U.S. Patent 5,278,282.
(5) Yeh, T. F.; Reiser, A.; Dammel, R. R.; Pawlowski, G.; Roeschert, H. *Macromolecules* **1993**, *26*, 3862.
(6) Wielgolinski, L. *Polym. Prepr.* **1991**, 32 (2), 15.
(7) Ueberreiter, K. The Solution Process. In *Diffusion in Polymers*; Crank, J., Park, G. S., Eds.; Academic Press: New York, 1968.
(8) Ueberreiter, K.; Asmussen, F. *J. Polym. Sci.* **1962**, *57*, 187.
(9) Asmussen, F.; Ueberreiter, K. *J. Polym. Sci.* **1962**, *57*, 199.
(10) Narasimhan, B.; Peppas, N. A. *Adv. Polym. Sci.* **1997**, *128*, 157.
(11) Tu, Y. O.; Ouano, A. C. *IBM J. Res. Dev.* **1977**, *21*, 131.
(12) Devotta, I.; Ambeskar, V. D.; Mandhare, A. B.; Mashelkar, R. A. *Chem. Eng. Sci.* **1994**, *49*, 645.
(13) Ranade, V. V.; Mashelkar, R. A. *AIChE J.* **1995**, *41*, 666.
(14) Devotta, I.; Badiger, M. V.; Rajamohanan, P. R.; Ganapathy, S.; Mashelkar, R. A. *Chem. Eng. Sci.* **1995**, *50*, 2557.
(15) Lee, P. I.; Peppas, N. A. *J. Controlled Release* **1987**, *6*, 201.
(16) Brochard, F.; de Gennes, P.-G. *Phys. Chem. Hydrodyn.* **1983**, *4*, 313.
(17) Herman, M. F.; Edwards, S. F. *Macromolecules* **1990**, *23*, 3662.
(18) Papanu, J. S.; Soane, D. S.; Bell, A. T.; Hess, D. W. *J. Appl. Polym. Sci.* **1989**, *38*, 859.
(19) Peppas, N. A.; Wu, J. C.; von Meerwall, E. D. *Macromolecules* **1994**, *27*, 5626.
(20) Narasimhan, B.; Peppas, N. A. *J. Polym. Sci., Polym. Phys. Ed.* **1996**, *34*, 947.
(21) Narasimhan, B.; Peppas, N. A. *Macromolecules* **1996**, *29*, 3283.
(22) Papanu, J. S.; Hess, D. W.; Soane, D. S.; Bell, A. T. *J. Electrochem. Soc.* **1989**, *136*, 3077.
(23) Rodriguez, F.; Krasicky, P. D.; Groele, R. J. *Solid State Technol.* **1985**, *28*, 125.
(24) Rao, V.; Kosbar, L. L.; Frank, C. W.; Pease, R. F. W. *Proc. SPIE* **1991**, *1672*, 214.
(25) Blackadder, D. A.; Le Poidevin, G. J. *Polymer* **1978**, *19*, 483.
(26) Ouano, A. C.; Carothers, J. A. *Polym. Eng. Sci.* **1980**, *20*, 160.
(27) Papanu, J. S.; Hess, D. W.; Soane, D. S.; Bell, A. T. *J. Electrochem. Soc.* **1989**, *136*, 1195.
(28) Gadian, D. G. In *NMR and its Applications to Living Systems*; Oxford University Press: Oxford, 1995.
(29) Blumich, B., Kuhn, W., Eds. *Magnetic Resonance Microscopy*; VCH: Weinheim, 1992.
(30) Blumer, P., Blumich, B., Botto, R., Fukushima, E., Eds. *Spatially Resolved Magnetic Resonance*; Wiley-VCH: Weinheim, 1998.
(31) Shibuya, T.; Yasunaga, H.; Kurosu, H.; Ando, I. *Macromolecules* **1995**, *28*, 4377.
(32) Britton, M. M.; Callaghan, P. T. *J. Rheol.* **1997**, *41*, 1365.
(33) McDonald, P. J. *Prog. Nucl. Magn. Reson. Spectrosc.* **1997**, *30*, 69.
(34) Morris, P. G. In *Nuclear Magnetic Resonance Imaging in Medicine and Biology*; Clarendon Press: Oxford, 1986.
(35) Peppas, N. A.; Narasimhan, B.; Snaar, J. E. M.; Bowtell, R. W.; Melia, C. D. *Proc. Int. Symp. Controlled Release Bioact. Mater.* **1997**, *24*, 171.
(36) Duda, J. L.; Vrentas, J. S.; Ju, S. T.; Liu, T. *AIChE J.* **1982**, *28*, 279.
(37) Flory, P. J.; Rehner, Jr., J. *J. Chem. Phys.* **1943**, *11*, 521.
(38) Vrentas, J. S.; Vrentas, C. M. *Macromolecules* **1993**, *26*, 6129.
(39) Vrentas, J. S.; Vrentas, C. M. *Eur. Polym. J.* **1998**, *26*, 6129.
(40) De Gennes, P.-G. *J. Chem. Phys.* **1971**, *55*, 571.
(41) De Gennes, P.-G. In *Scaling Concepts in Polymer Physics*; Cornell University Press: Ithaca, NY, 1979.
(42) Doi, M.; Edwards, S. F. In *The Theory of Polymer Dynamics*; Clarendon Press: Oxford, 1986.
(43) Mallapragada, S. K.; Peppas, N. A. *J. Polym. Sci., Polym. Phys. Ed.* **1996**, *34*, 1339.
(44) Bowtell, R. W.; Sharp, J. C.; Peters, A.; Mansfield, P.; Rajabi-Siahboomi, A. R.; Davies, M. C.; Melia, C. D. *Magn. Reson. Imaging* **1994**, *12* (2), 361.
(45) Bowtell, R. W.; Robyr, P. *J. Magn. Reson.* **1998**, *131*, 286.
(46) Edelstein, W. A.; Hutchinson, J. M. S.; Johnson, G.; Redpath, T. *Phys. Med. Biol.* **1980**, *25*, 751.
(47) Parsonage, E. E.; Peppas, N. A. *Br. Polym. J.* **1987**, *19*, 469.
(48) Lustig, S. R.; Caruthers, J. M.; Peppas, N. A. *Chem. Eng. Sci.* **1992**, *47*, 3037.
(49) Crank, J. In *Free and Moving Boundary Problems*; Oxford University Press: New York, 1984.
(50) Hoffman, J. D. In *Numerical Methods for Engineers and Scientists*; McGraw-Hill: New York, 1992.
(51) Blum, F. D.; Durairaj, B.; Padmanabhan, A. S. *J. Polym. Sci., Polym. Phys. Ed.* **1986**, *24*, 493.
(52) Tirrell, M. *Rubber Chem. Technol.* **1984**, *57*, 523.
(53) Klein, J. *Nature* **1978**, *271*, 143.
(54) Bartels, C. R.; Graessley, W. W.; Crist, B. *J. Polym. Sci., Polym. Lett.* **1983**, *21*, 495.

MA981382K